Inverse Design of Scaffolds for Bone Tissue Engineering using Artificial Neural Networks and Generative Additive Models

Aadi Bhensdadia[1], Silvia Ibrahimi[2], Francesco Maffezzoli[2], Massimo W. Rivolta[2]

***Abstract*— Scaffold design for bone tissue engineering along with recent advances in 3D printing represents a major technology to promote the healing of critical bone defects. However, designing the scaffold geometry from a given set of desired properties is challenging and typically tackled by means of high-complexity finite element simulations. Recently, the use of artificial neural networks (ANNs) has started emerging in this field and has provided promising results. In this study, we investigated the development of an ANN to predict the design parameters of a specific geometrical structure from the family of Triply-Periodic Minimal Surfaces, i.e., the gyroid. Unlike other studies, we investigated i) the possibility of using only morphological characteristics of the scaffold to predict the design parameters; ii) the prediction of anisotropic scaffolds since anisotropy has been found to significantly improve bone regeneration; and iii) the comparison of the performance of the ANN with a generalized additive model (GAM) previously designed for the same task. We generated a synthetic dataset of 6940 gyroids where the 90% was used to train the models and 10% for performance evaluation. A feature selection procedure was implemented to select the optimal feature set for the prediction. With the same feature set, the ANN outperformed the GAM in the prediction of all design parameters with Pearson's correlation coefficients ranging from 0.53 to 0.82, while the GAM's ranged from 0.41 to 0.51. The ANN also displayed a lower mean absolute error than GAM. The results of the study support the use of ANN for scaffold design. Further evaluations are needed to assess the feasibility of this technology in clinical applications.**

I. INTRODUCTION

Severe bone defects and injuries often require additional structural reinforcement to promote effective tissue regeneration. With recent advances in 3D printing, a novel approach has emerged for addressing bone defects: scaffold design for tissue engineering. These scaffolds can exhibit a wide range of architectures, from randomly distributed structures to organized porous designs, such as Triply-Periodic Minimal Surfaces (TPMS) [1]. Estimating the mechanical and morphological properties of these scaffolds during the design phase is essential but typically relies on time-consuming methods like finite element analysis [2] and image processing. In practical applications, solving the inverse problem, *i.e.*, determining scaffold geometrical parameters based on a set of desired mechanical and morphological features, is often more relevant, as it allows clinicians and engineers to obtain a ready-to-print prototype for implantation in patients.

Several studies have tackled the problem of inverse design of TPMS scaffolds using several computational intelligence techniques, including artificial neural networks (ANN) [3], genetic algorithms [4], or Convolutional Neural Networks (CNN) [5]. Generative approaches such as generative adversarial networks or variational autoencoders [6] have also been explored. Most studies have focused on designing isotropic scaffolds optimized for specific mechanical properties, such as the stiffness matrix or Young's modulus.

In our previous work [7], we investigated on the link between scaffold features and effective inverse designs using a generalized additive model (GAM) which was inspired by the modern Residual Net architectures in Deep Learning. The proposed model achieved good predictions in determining the geometrical parameters of three TPMS scaffolds by means of a set of mechanical and morphological features, which most impacted the performance of the inverse model.

To the best of our knowledge, prior studies have primarily focused on perfectly isotropic TPMS structures or have mostly used mechanical properties as target features for inverse design. In this work, we tested whether an ANN could solve the inverse problem for anisotropic TPMS scaffolds. In addition, we wanted to verify whether morphological features alone could achieve a good prediction of scaffold morphological parameters. To do so, we first extracted morphological features from a newly generated scaffold dataset and performed feature selection. Finally, we benchmarked the trained ANN with our previous GAM retrained on the features extracted from these anisotropic scaffolds.

II. METHODS

A. Dataset

A custom-made dataset was developed using the gyroid geometry of the TPMS architectures. The gyroid geometry was selected due to its favorable regeneration-aiding characteristics; it displays a close similarity to the bone trabeculae, preventing stress concentration and allowing for retention of good mechanical properties in the long-term [8]. Briefly, the gyroid surface was defined using the following implicit function sampled at discrete position x, y and z:

$$f(x,y,z) = \sin(k_x x)\cos(k_y y) + \sin(k_y y)\cos(k_z z) + \sin(k_z z)\cos(k_x x) + b \quad (1)$$

*This study was partially carried out within the project "Artificial Intelligence-based design of 3D PRINTed scaffolds for the repair of critical-sized BONE defects" I-PRINT-MY-BONE funded by European Union - Next Generation EU within the PRIN 2022 program (D.D. 104 - 02/02/2022 Ministero dell'Università e della Ricerca), Mission 4, Component 1, CUP D53D23003390006.

[1]AB is at Pine View School, 1 Python Path, Osprey, FL, 34229, United States

[2]SI, FM and MWR are with the Dipartimento di Informatica "Giovanni Degli Antoni", Università degli Studi di Milano, Via Celoria 18, Milan, 20133, Italy

Corresponding author: aadibhensdadia@gmail.com

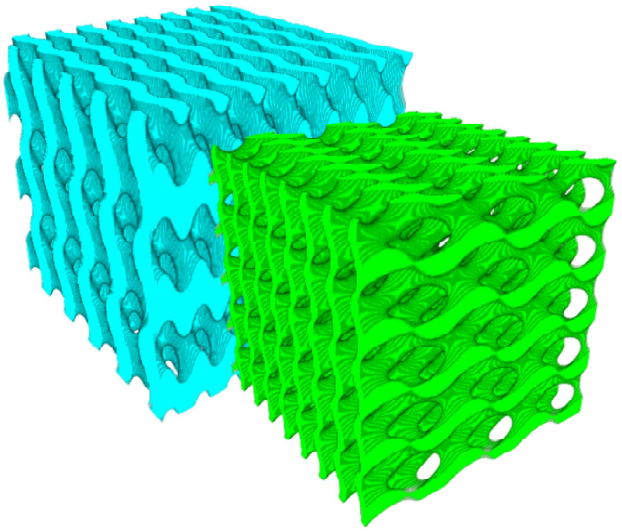

Fig. 1: Example of two anisotropic scaffolds generated with different combinations of parameters.

where $k_i = 2\pi r_i/n$, r_i is the number of repetitive units along dimension i controlling the anisotropy of the scaffold, n is the number of voxels per edge, b controls the gyroid surface and x, y, z ranged from 1 to n. We set $n = 300$, and $r_i = 3, 5, 8$.

In order to create a volume, a binary cube with shape (n, n, n) was created. Voxels were considered solid if the following condition was satisfied:

$$|f(x, y, z)| < \delta \tag{2}$$

where δ controls the volume generated from the surface [9].

A dataset of scaffolds was created by varying the b parameter from 0 to 2 with a step of 0.1, and the δ parameter from 0.4 to 1.5, with a step of 0.05. For each combination of (b, δ) parameters, 27 scaffolds were generated by changing r_x, r_y, and r_z between their 3 possible values. In this way, the dataset contained scaffolds with asymmetric properties along their axes, introducing an anisotropic factor as shown in Fig. 1.

Scaffolds were excluded from the dataset if they fulfilled either of the following characteristics:

- Pores were completely disconnected at any point: this occurred when pores were separated by a fully solid layer of voxels at any layer. These scaffolds would not effectively allow the movement of nutrients between cells, thus inhibiting tissue growth.
- For various combinations of parameters, the scaffold would be either completely solid or empty.

After applying these filtering criteria, 6940 anisotropic scaffolds remained in the dataset.

B. Feature Extraction

A total of 11 morphological features were extracted from each scaffold: barycenter (x_c, y_c, z_c), surface-to-volume ratio (s/v), volumetric fraction (ρ), mean, maximum, and standard deviation of trabecular thickness ($Tb.Th._{mean}$, $Tb.Th._{max}$, $Tb.Th._{std}$) and mean, maximum, and standard deviation trabecular spacing ($Tb.Sp._{mean}$, $Tb.Sp._{max}$, $Tb.Sp._{std}$).

Barycenter, surface-to-volume, and volumetric fraction features were extracted using custom-made Python scripts. Trabecular thickness and spacing features were instead extracted using the BoneJ plugin [10] of ImageJ [11]. A custom ImageJ macro processed all scaffolds.

C. Models

The relationship between the design parameters and the extracted morphological features were generally nonlinear in nature, making machine learning regression a viable method to solve the inverse problem. We initially developed a fully-connected ANN with a 11-dimensional column vector $\mathbf{x}$ as input, containing all parameters extracted as mentioned above. The ANN outputted a 5-dimensional vector $\hat{\mathbf{y}}$, representing the estimate of the design parameters. Given the target geometrical features:

$$\mathbf{y} = [b, \delta, r_x, r_y, r_z]^\intercal \tag{3}$$

its prediction was hence $\hat{\mathbf{y}}$.

The ANN was composed of three fully-connected hidden layers, each of which was separated by exponential learning unit activations (default value $\alpha = 1$ used). In order to optimize the ANN's parameter vector θ, the mean squared error (MSE) between the target and predicted geometrical features was minimized using the Adam optimizer. Defining the ANN as: $\hat{\mathbf{y}} = m_\theta(\mathbf{x})$, the loss function was:

$$L(\theta) = \mathbb{E}_{(\mathbf{x},\mathbf{y})\sim p_{\text{data}}}\left[(\mathbf{y} - m_\theta(\mathbf{x}))^2\right] \tag{4}$$

where $\mathbb{E}$ is the expected value computed over the samples within a minibatch and p_{data} is the distribution of the dataset.

In our previous work [7], we developed a GAM to tackle the scaffold inverse problem. In this study, this model was adapted to solve the inverse problem for anisotropic gyroids and by changing the input features. Briefly, the model was a linear combination of each feature with an additional non-linear component:

$$\hat{y}_k = c_k + \mathbf{w}_{1,k}^\intercal \mathbf{x} + \mathbf{w}_{2,k}^\intercal \tanh(\text{diag}(\mathbf{w}_{3,k})\mathbf{x} + \mathbf{w}_{4,k}) \tag{5}$$

where $\hat{y}_k$ is the k-th entry of the vector $\hat{\mathbf{y}}$, $\mathbf{w}_{j,k}$ and c_k represent the model parameters, $\text{diag}(\mathbf{z})$ constructs a diagonal matrix with the element of $\mathbf{z}$ on its diagonal, and $\tanh(\mathbf{z})$ is applied point-wise to the element of $\mathbf{z}$. By construction, this model also allowed the total prediction of each feature $\hat{y}_k$ to be expressed as a sum of independent terms $\Delta\hat{y}_{k,i}$, granting the additive property to the model:

$$\begin{aligned} \hat{y}_k &= c_k + \sum_i \Delta\hat{y}_{k,i} \\ \Delta y_{k,i} &= w_{1,k,i} x_i + w_{2,k,i} \tanh(w_{3,k,i} x_i + w_{4,k,i}) \end{aligned} \tag{6}$$

where x_i is the i-th entry of the feature vector $\mathbf{x}$.

Similarly to ANN training, the model parameters were optimized by minimizing the MSE between the target and the predicted features using the Adam optimizer.

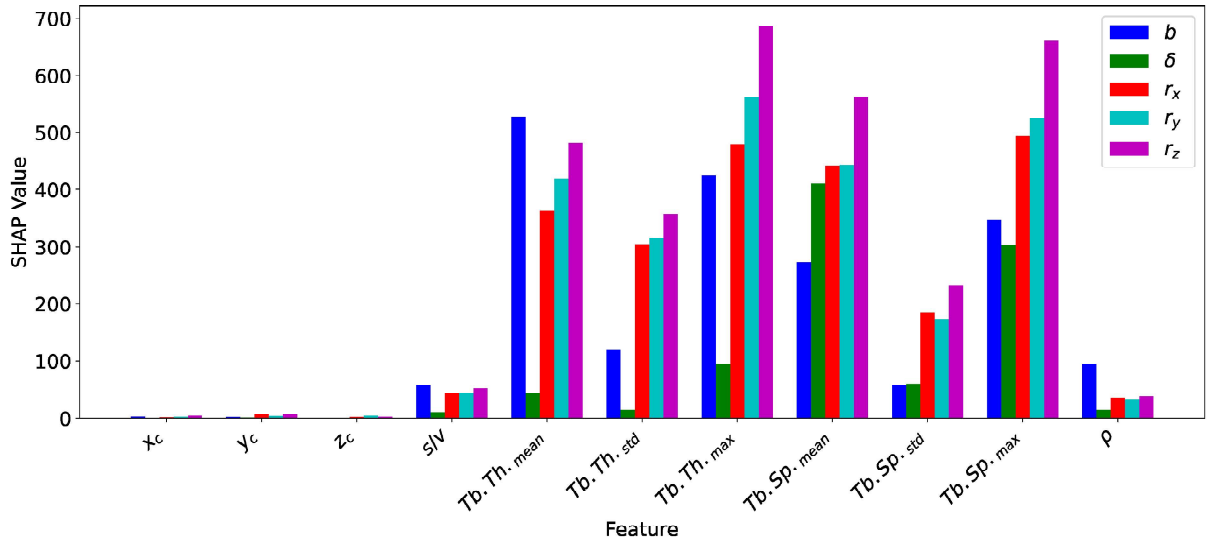

Fig. 2: SHAP values of all features for each design parameter.

D. Hyperparameter Tuning and Feature Selection

The dataset was randomly divided into training, validation, and test set for training and performance evaluation. The training-validation-test split was 80-10-10, yielding to 5554, 693, and 693 scaffolds in each dataset, respectively. c The ANN was trained for 75 epochs to optimize model performance. The number of epochs was determined by training multiple ANN models with the same model architecture, iterating from 5 to 100 epochs. The effect of the number of epochs on model performance was quantified by the Pearson's correlation coefficients between the predicted and ground truth values of b, δ, r_x, r_y, and r_z on the validation set. Here, we found that increasing the number of epochs beyond 75 did not significantly improve the performance of the model.

The model architecture was selected among 7 different architectures by comparing the performance achieved on the validation set. The final architecture mapped the 11 input features to the 5 output design parameters with 3 hidden layers in between, of respectively 128, 256, and 64 neurons. The learning rate was fixed at 10^{-4}, which is very commonly used with the Adam optimizer.

A feature selection procedure was implemented to detect the most influential features for the prediction of the design parameters. The use of all 11 parameters could be not only unnecessary for prediction, but also impractical from an engineering perspective. Here, we used SHapley Additive exPlantations (SHAP) to detect the most important features after the training of the ANN model. All SHAP values were calculated from the validation set. Since SHAP values did not account for possible correlations between the input features, we computed the correlations between pairs of features. If two features had a Pearson's correlation coefficient > 0.70, we removed the one with lower average SHAP value across the 5 outputs.

As a last step, we trained the final ANN and GAM on the selected feature vectors, using the same dataset splits, and compared their performance.

III. RESULTS AND DISCUSSIONS

Regarding the feature selection, as can be seen in the Fig. 2, the barycenter features (x_c, y_c, z_c), the surface-to-volume ratio (s/v), and volumetric fraction (ρ) parameters had SHAP values that were significantly lower than the others. For this reason, they were the first ones to be discarded. In the case of $Tb.Th._{mean}$ and $Tb.Th._{max}$, which had a correlation coefficient of 0.93, $Tb.Th._{max}$ had a slightly higher average SHAP value across all design parameters, at 376 as opposed to $Tb.Th._{mean}$, at 347. $Tb.Sp._{mean}$ and $Tb.Sp._{max}$ had a correlation coefficient of 0.95, but $Tb.Sp._{max}$ had a higher average SHAP value, at 548 compared to 487 for $Tb.Sp._{mean}$. This led to the discardment of $Tb.Th._{mean}$ and $Tb.Sp._{mean}$, leaving us with 4 input features.

As expected, the trabecular thickness and spacing played an important role in predicting the values of b and δ. Interestingly, they also supported the prediction of r_x, r_y and r_z, even though thickness and spacing were global properties of the scaffold and not specifically dependent on the porous directions. The barycenter did not play any significant role.

	Person's correlation coefficient				
Model name	b	δ	r_x	r_y	r_z
ANN	0.82	0.73	0.54	0.53	0.54
GAM	0.51	0.49	0.41	0.45	0.46
	MAE				
Model name	b	δ	r_x	r_y	r_z
ANN	0.28	0.18	1.41	1.48	1.44
GAM	0.50	0.26	1.61	1.53	1.59

TABLE I: Pearson's correlation coefficient and MAE for both models and all design parameters.

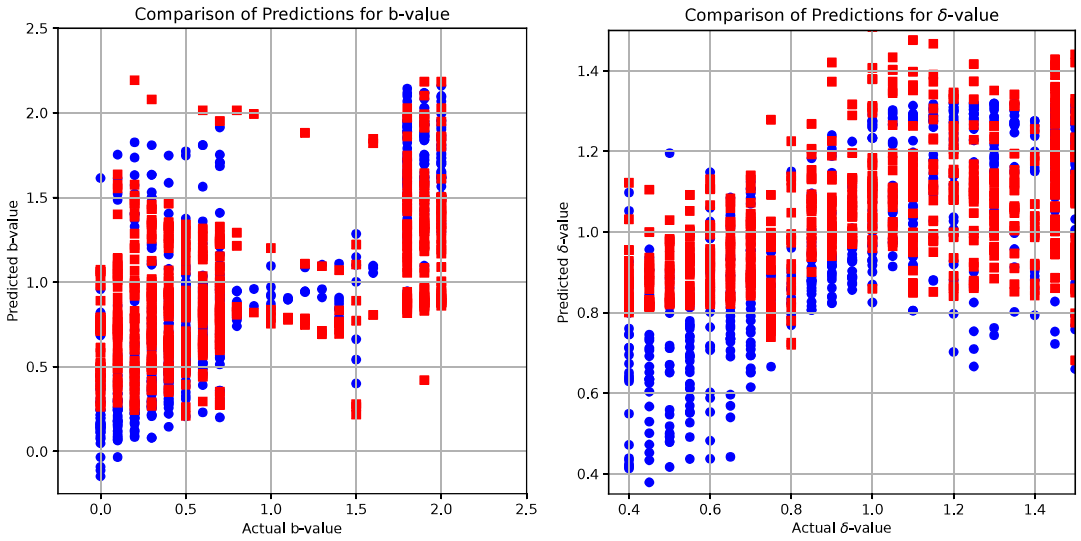

(a) (b)

Fig. 3: Scatterplot for both models for (a) b value; and (b) δ value. Blue dots refer to the ANN model, while red squares refer to the GAM model.

These results were expected since the gyroid geometry considered had a symmetrical and periodical structure ($n = 300$ and x, y and z had maximum value of 300) even in presence of different repetitive units along its three axes. Finally, the surface-to-volume ratio and volumetric fraction brought minor contributions in predicting the design parameters. These results hinted that there were many scaffolds with different design parameters with similar s/v and ρ.

It is worth mentioning that the morphological anisotropy could be directly set using the gyroid parameters r_x, r_y and r_z, and their prediction might not be needed for this TPMS scaffold in practice. Our results showed that the anisotropy could be predicted from morphological parameters and this observation can be leveraged in scaffolds where no direct parameters control the anisotropy.

The final ANN and GAM with 4-feature inputs were evaluated using Pearson's correlation coefficient and mean absolute error (MAE) on the testing dataset between the ground truth b, δ, r_x, r_y and r_z and their predicted values. The ANN achieved higher performance on all design parameters for both metrics than the GAM. The results suggested that not only ANN better followed the trend of the parameters but also achieved a lower bias. Both metrics are reported in Table I, while the scatterplots for prediction of b and δ values are reported in Fig. 3.

As supported by the results, the performance of the ANN was significantly better than GAM's in solving the inverse problem. The main reason was likely due to the large difference in the number of parameters of the two models, which made the ANN more flexible and better fit the data distribution. The GAM required the training of 145 parameters while the ANN had more than 50 thousand. However, the decomposition property of GAM may enable a clear understanding of the contribution of each feature to the final prediction of each scaffold parameter, which might be useful for explaining the model's predictions. For the ANN, this was not possible.

Another important difference with respect to our previous work was that, in this study, we used only morphological features of the scaffold for the prediction. This may explain the performance drop achieved here by GAM, as mechanical features may also contribute to the optimal prediction of b and δ [7]. Our objective was to assess the feasibility of using morphological features only in an anisotropic setting; however, it is worth noting that the higher prediction in design parameters (specifically, b and δ) achieved by ANN could be not necessarily associated to an optimal scaffold design if specific mechanical properties are requested as well. Future works will study the impact of the use of only morphological features on the mechanical properties of the scaffold.

IV. CONCLUSIONS

The purpose of this study was to develop an ANN that was able to tackle the inverse design problem for TPMS scaffolds for bone tissue engineering that accounted for desired morphological properties and anisotropy, and compare its performance with an existing model developed in our previous work.

Anisotropic scaffolds have been found to significantly improve trabecular bone regeneration. Although further development is needed for our models, this study is a step forward in the design and clinical application of bone scaffolds that may have a greater potential for trabecular regeneration over existing designs, improving the quality of care for patients with critical bone defects.

REFERENCES

[1] X. Zheng, Z. Fu, K. Du, C. Wang, and Y. Yi, "Minimal surface designs for porous materials: from microstructures to mechanical properties," *Journal of Materials Science*, vol. 53, no. 14, pp. 10 194–10 208, 2018.

[2] A. Boccaccio, A. Ballini, C. Pappalettere, D. Tullo, S. Cantore, and A. Desiate, "Finite element method (fem), mechanobiology and biomimetic scaffolds in bone tissue engineering." *International journal of biological sciences*, vol. 7, pp. 112–32, Jan 2011.

[3] D. Patel, R. Yang, J. Wang, R. Rai, and G. Dargush, "Deep learning-based inverse design framework for property targeted novel architectured interpenetrating phase composites," *Composite Structures*, vol. 312, p. 116783, 2023.

[4] W. Liu, Y. Zhang, Y. Lyu, S. Bosiakov, and Y. Liu, "Inverse design of anisotropic bone scaffold based on machine learning and regenerative genetic algorithm," *Frontiers in Bioengineering and Biotechnology*, vol. 11, p. 1241151, 2023.

[5] A. Viswanath, D. W. Abueidda, M. Modrek, R. K. Abu Al-Rub, S. Koric, and K. A. Khan, "Designing a tpms metamaterial via deep learning and topology optimization," *Frontiers in Mechanical Engineering*, vol. 10, p. 1417606, 2024.

[6] Y. Liu, H. He, Y. Cao, Y. Liang, and J. Huang, "Inverse design of tpms piezoelectric metamaterial based on deep learning," *Mechanics of Materials*, vol. 198, p. 105109, 2024.

[7] S. Ibrahimi, L. D'Andrea, D. Gastaldi, M. W. Rivolta, and P. Vena, "Machine learning approaches for the design of biomechanically compatible bone tissue engineering scaffolds," *Computer Methods in Applied Mechanics and Engineering*, vol. 423, p. 116842, 2024.

[8] J. Ma, Y. Li, Y. Mi, Q. Gong, P. Zhang, B. Meng, J. Wang, J. Wang, and Y. Fan, "Novel 3d printed tpms scaffolds: microstructure, characteristics and applications in bone regeneration," *Journal of Tissue Engineering*, vol. 15, p. 20417314241263689, 2024, pMID: 38911101.

[9] R. Pugliese and S. Graziosi, "Biomimetic scaffolds using triply periodic minimal surface-based porous structures for biomedical applications," *SLAS technology*, vol. 28, no. 3, pp. 165–182, 2023.

[10] M. Doube, M. M. Kłosowski, I. Arganda-Carreras, F. P. Cordelières, R. P. Dougherty, J. S. Jackson, B. Schmid, J. R. Hutchinson, and S. J. Shefelbine, "Bonej: Free and extensible bone image analysis in imagej," *Bone*, vol. 47, no. 6, pp. 1076–1079, 2010.

[11] C. A. Schneider, W. S. Rasband, and K. W. Eliceiri, "Nih image to imagej: 25 years of image analysis," *Nature Methods*, vol. 9, no. 7, p. 671–675, 2012.